Journal of Geosciences, 65 (2020), 141–152 DOI: 10.3190/jgeosci.306

Original paper

Stangersite, a new tin germanium sulfide, from the Kateřina mine, Radvanice near Trutnov, Czech Republic

Jiří SEJKORA[1*], Emil MAKOVICKY[2], Tonči BALIĆ-ŽUNIĆ[2], Peter BERLEPSCH[3]

[1] *Department of Mineralogy and Petrology, National Museum, Cirkusová 1740, 193 00 Praha 9-Horní Počernice, Czech Republic; jiri.sejkora@nm.cz*
[2] *Institute for Geoscience and Natural Resources Management, University of Copenhagen, Østervolgade 10, DK-1350, Copenhagen K, Denmark*
[3] *Heinrichsgasse 8, 4055 Basel, Switzerland*
[*] *Corresponding author*

The new mineral stangersite was found in the burning waste dump of abandoned Kateřina coal mine at Radvanice near Trutnov, northern Bohemia, Czech Republic. The new mineral occurs as well-formed, flattened, acicular crystals with a cross-section of 2–5 × 20–40 μm and up to 1 cm in length. They constitute random or fan-shaped clusters on rock fragments and on crumbly black ash in association with greenockite, herzenbergite, unnamed GeS_2 and GeAsS. Stangersite was also observed as irregular grains, up to 100 μm in size, in the multicomponent aggregates on which the above-described crystals grow. These aggregates are formed, beside stangersite, by minerals of Bi–Sb, Bi_2S_3–Sb_2S_3 and Bi_2S_3–Bi_2Se_3 solid solutions, Bi_3S_2, Bi-sulfo/seleno/tellurides, tellurium, unnamed $PbGeS_3$, Cd_4GeS_6, GeAsS, GeS_2, $Sn_5Sb_3S_7$, greenockite, cadmoindite, herzenbergite, teallite and Sn- and/or Se-bearing galena. Stangersite formed under reducing conditions by direct crystallization from hot gasses (250–350 °C) containing Cl and F, at a depth of 30–60 cm under the surface of the dump. The mine dump fire started spontaneously and no anthropogenic material was deposited there. Stangersite is brittle (aggregates) or elastic, to flexible (acicular crystals). It is orange to yellowish red with a very light yellowish brown streak, translucent to transparent in transmitted light, and has vitreous to adamantine luster. Cleavage is perfect in two directions: perpendicular and oblique to elongation of crystals. The VHN microhardness is 55 $kp \cdot mm^{-2}$ (539 MPa) and corresponds to Mohs hardness about 2; the calculated density is 3.98 $g \cdot cm^{-3}$. In the reflected light, stangersite is light greyish white. Bireflectance and pleochroism were not observed due to distinct orange-brown internal reflections. Anisotropy under crossed polars is strong with dark brownish grey to reddish-brown or brownish violet rotation tints. The empirical formula, based on electron-microprobe analyses of acicular crystals of stangersite, is $Sn_{1.02}Ge_{0.94}(S_{2.93}Se_{0.10})_{\Sigma 3.03}$. The ideal formula is $SnGeS_3$, which requires Sn 41.29, Ge 25.25, S 33.46, total 100 wt. %. The chemical composition of stangersite from multicomponent aggregates shows an extensive $PbSn_{-1}$ substitution covering nearly the whole field of stangersite in the $SnGeS_3$–$PbGeS_3$ solid solution. Stangersite is monoclinic, $P2_1/c$, $a = 7.2704(15)$, $b = 10.197(2)$, $c = 6.8463(14)$ Å, $\beta = 105.34(3)^\circ$, with $V = 489.5$ Å^3 and $Z = 4$. The strongest reflections of the powder X-ray diffraction pattern [*d*, Å/I(*hkl*)] are: 7.006/100(100), 4.135/49(120), 3.077/47(130), 2.776/38(022), 2.699/69(211), 2.1213/31(320), and 1.7239/35(41–2; 410). Stangersite has a layered structure, with corrugated (100) layers of $Sn^{2+}S_5$ coordination pyramids and with interspaces filled by lone electron pairs of Sn^{2+} and [001] chains of $Ge^{4+}S_4$ coordination tetrahedra. The Raman spectrum of stangersite with tentative band assignments is given. We named the mineral after its chemical constituents: Sn (**stan**num), Ge (**ger**manium) and S (**s**ulphur).

Keywords: stangersite, new mineral, tin germanium sulfide, crystal structure, Raman spectroscopy, Radvanice
Received: 19 March 2020; accepted: 23 June 2020; handling editor: F. Laufek

1. Introduction

The burning mine dump of the Kateřina mine at Radvanice near Trutnov (Czech Republic) is the first locality of natural monoclinic $SnGeS_3$. First data about the burning dump of the Kateřina mine published Dubanský et al. (1988, 1991). First identification of $SnGeS_3$ from Radvanice was given by Žáček and Ondruš (1997a,b) and later was confirmed by Tvrdý and Sejkora (1999, 2000). The results of a detailed mineralogical study and refinement of the $SnGeS_3$ crystal structure were published by Sejkora et al. (2001). At that time, strict rules of the Commission on New Minerals and Mineral Names of the International Mineralogical Association (CNMMN-IMA) did not allow submission of this natural phase as a valid mineral species (Nickel and Grice 1998): *"It has therefore been decided that, as a general rule, products of combustion are not to be considered as minerals in the future."*). The recent change of rules (Miyawaki et al. 2019) regarding combustion products forming on burning coal dumps allows now a description of crystal phases forming on the burning coal dumps with no human agency initiating the fire and no anthropogenic material deposited as minerals (CNMNC-IMA proposal 16-F). Therefore, the new mineral and the name were approved by the Commission on New Minerals, Nomenclature and Classification of the International Mineralogical Association (IMA 2019-092). The holotype specimen of stangersite is deposited in the collections of the Department of Mineralogy and Petrology, National Museum in Prague, Cirkusová 1740, 19300 Praha 9, Czech Republic under the catalog number P1P 8/2000. The name of mineral (stangersite) is related to its chemical constituents: Sn (**stan**num), Ge (**ger**manium) and S (**s**ulfur).

2. Occurrence

Stangersite samples were found in 1995–1998 in the central part of a burning coal mine dump of abandoned Kateřina coal mine (GPS: 50°33'39.0"N 16°03'56.2"E), situated at the eastern part of the Radvanice village, about 12 km east of the district town of Trutnov (northern Bohemia, Czech Republic). At this mine dump, mine wastes from the former Kateřina mine were deposited for over 100 years. Their total volume was estimated to be 2.331×10^6 m^3 (Osner and Němec 2002). In the past, coal was there only hand-picked, and the coal of the low-quality was deposited on the dump, and therefore dump material contained 19 vol. % on average and locally up to 40 vol. % of coal (Laufek et al. 2017). Later, during uranium mining at the Kateřina mine, all non-mineralized coal and coal-bearing claystone (locally abundant in sulfides) were deposited in this mine dump. The mine dump caught fire spontaneously before 1967 and culminated between 1980–1981 (Dubanský et al. 1991; Osner and Němec 2002). Temperatures in this burning dump reached up to 1000 °C or more. Due to possible ecological hazards for the Radvanice village, the Czech government decided to liquidate and remediate this mine dump. The work started in 1998 and was successfully completed in 2005 (Osner and Němec 2002; Žáček and Skála 2015; Laufek et al. 2017).

In the Kateřina mine area, six coal measures are known; the thickness of the measures exploited reached up to 1 m, exceptionally 1.5–1.9 m. The coal-bearing sediments belong to Odolov member of the Jívka Formation (age of Stephanian–B), belonging to the Czech limb of the Intrasudetic Basin. This basin comprises sediments from early Pennsylvanian (Namurian) up to the Lower Triassic (Tásler et al. 1979). The characteristic feature of the Radvanice coals and surrounding sediments is their mineralization and enrichment in Se, Mo, As, Pb, Cu, Zn, Ge, U, Cd, Sb, Bi and other elements (Kudělásek 1959a, b; Čadková 1971). The increased contents of some elements in coal-bearing sediments have been studied since 1945. Besides experiments in copper and germanium extraction, the uranium mineralization (uraninite and coffinite) was mined in the years 1952–1957. After 1957 only coal was mined again, and in 1993 all mines in the Radvanice area were closed.

Stangersite was found in a part of mine dump within an area of 2 m^2 and about 30–60 cm under the surface of the mine dump. The temperature reached up 350 °C at this place. Rich crusts were reaching the thickness of about 10–15 cm at some places and formed by sal ammoniac, cryptohalite and bararite, besides sulfur and dark orange amorphous As-rich sulfur, developed above the horizon with Sn–Ge mineral phases. Two types of stangersite occurrences were observed in the studied material. The first type represents well-formed, acicular, lath-like crystals. They are in the association with greenockite, herzenbergite, and unnamed phases GeS_2 and GeAsS. The second type is represented by irregular stangersite grains deposited in multicomponent aggregates. The above-described crystals grow on those aggre-

Fig. 1 Stangersite: flattened acicular crystals on the surface of a rock fragment; Radvanice, horizontal field of view 3 mm, photo J. Sejkora.

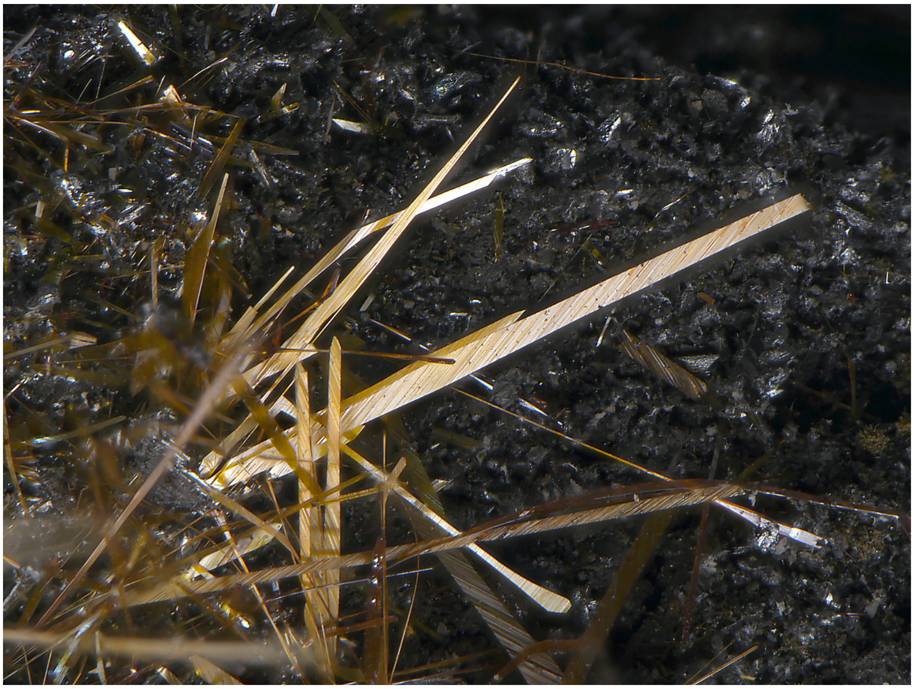

Fig. 2 Clusters of flattened acicular crystals of stangersite on the surface of rock fragments; Radvanice, horizontal field of view 4 mm, photo J. Sejkora.

gates. The following phases were detected to be closely associated: members of Bi–Sb, Bi_2S_3–Sb_2S_3 and Bi_2S_3–Bi_2Se_3 solid solutions, Bi_3S_2, Bi-sulfo/seleno/tellurides, tellurium, unnamed $PbGeS_3$, Cd_4GeS_6, GeAsS, GeS_2, $Sn_5Sb_3S_7$, greenockite, cadmoindite, herzenbergite, teallite and Sn- and/or Se-bearing galena. Stangersite formed very likely under reducing conditions by direct crystallization from hot gasses (250–350 °C) containing Cl and F at a depth of 30–60 cm under the surface of a burning coal mine dump.

Monoclinic synthetic phases of the $SnGeS_3$–$PbGeS_3$ series have been known long before they were found in nature. $SnGeS_3$ was studied by Bente (1975), Öztunali and Moh (1980) and many others, especially with regard to its vibrational and photoelectric properties. The crystal structure of synthetic $SnGeS_3$, was described by Fenner and Mootz (1974, 1976). Fenner and Mootz (1976) synthesized single crystals of $SnGeS_3$ by various methods – hydrothermal (at 450 °C), from the melt (at 500 °C), and also by vapor-phase transport (at 565–485 °C). Later, Bente (1981) described a continuous solid-solution towards $PbGeS_3$ at 450 °C. More recently, Laufek et al. (2017) determined $SnGeS_3$ as a product of the experiment comprising a vapor-phase transport in the presence of sal ammoniac.

3. Physical and optical properties

As mentioned above, two morphological types of stangersite were observed in the studied material. The first type is represented by flattened acicular crystals with a cross-section of 2–5 × 20–40 μm and up to 1 cm in length (Fig. 1). They produce random or fan-shaped clusters growing on rock fragments and crumbly black ash (Fig. 2). The second type forms irregular grains, 2–100 μm in size, as a part of earlier multicomponent aggregates. Stangersite is orange to yellowish red with a very light yellowish brown streak. The mineral is translucent to transparent in transmitted light and has vitreous to adamantine luster. Cleavage is perfect in two directions, perpendicular and oblique to elongation of crystals. Tenacity is brittle (aggregates) or elastic, to flexible (acicular crystals). Calculated density ($Z = 4$) for the empirical formula and unit-cell volume refined from the single crystal data is 3.98 $g \cdot cm^{-3}$. The VHN microhardness of stangersite measured using PMT-3 microhardness tester with Vickers diamond pyramid and NaCl crystals as standard (load 10 g, 15 s) is 55 $kp \cdot mm^{-2}$ (539 MPa) and corresponds to the Mohs hardness of about 2. In the reflected light, stangersite is light greyish white,

Tab. 1 Reflectance values of stangersite (measured in air)

R_{max}	R_{min}	λ (nm)	R_{max}	R_{min}	λ (nm)
39.3	39.3	400	26.5	25.3	560
34.9	34.5	420	26.7	25.1	580
31.6	30.9	440	26.9	25.2	589 (COM)
29.5	28.7	460	27.3	25.6	600
28.7	27.8	470 (COM)	27.4	25.2	620
28.1	27.0	480	27.9	25.4	640
27.2	25.8	500	28.1	25.6	650 (COM)
26.4	25.1	520	28.2	25.2	660
26.2	25.0	540	28.9	25.7	680
26.2	25.0	546 (COM)	29.0	25.8	700

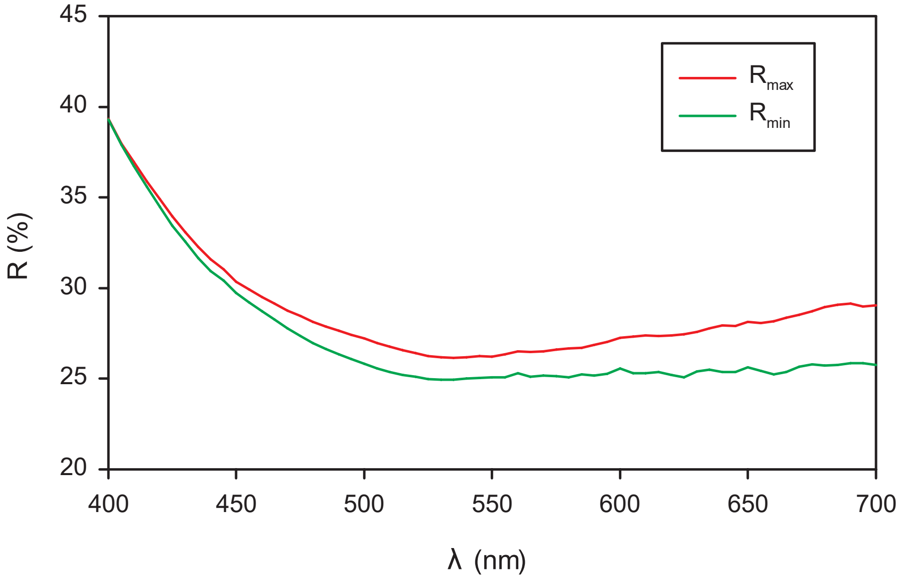

Fig. 3 Reflectivity curves for stangersite (in air).

bireflectance, or pleochroism not observed due to distinct orange-brown internal reflections. Anisotropy in crossed polars is strong with dark brownish grey to reddish-brown or brownish violet rotation tints. Reflectance percentages (air) for the four COM wavelengths (R_{min} and R_{max}) are: 27.8/28.7 (470 nm), 25.0/26.2 (546 nm), 25.2/26.9 (589 nm), and 25.6/28.1 (650 nm). The full set of reflectance

Tab. 2 Chemical data (in wt. %) for acicular crystals of stangersite (Sejkora et al. 2001)

Constituent	Mean	Range	Stand. dev.	Reference material
Sn	40.47	40.06–40.86	0.15	Sn
Pb	0.29	0.00–0.71	0.11	PbS
Ge	22.73	21.90–23.23	0.19	Ge
Fe	0.03	0.00–0.20	0.03	chalcopyrite
Bi	0.27	0.00–0.78	0.11	Bi
Sb	0.10	0.00–0.18	0.02	Sb_2Se_3
As	0.10	0.00–0.23	0.04	Cu_3AsS_4
S	31.42	30.73–32.18	0.23	chalcopyrite
Se	2.62	1.61–3.58	0.32	Sb_2Se_3
Total	98.03			

Tab. 3 Representative chemical analyses (in wt. %) for stangersite grains at multicomponent aggregates from Radvanice

	1	2	3	4	5	6	7	8	9	10	11	12
Sn	17.93	21.51	26.20	27.05	27.14	27.79	28.55	29.95	30.90	36.57	38.63	40.00
Pb	31.10	27.69	20.32	18.46	17.87	16.86	15.56	15.28	13.51	6.79	4.00	0.95
Cd	0.00	0.00	0.00	0.00	0.00	0.00	0.00	0.00	0.00	0.16	0.00	0.00
Ge	19.79	20.47	20.79	20.90	21.27	20.78	20.95	21.14	21.77	21.73	22.86	22.95
Sb	0.24	0.00	0.10	0.13	0.15	0.20	0.09	0.11	0.00	0.10	0.15	0.16
As	0.18	0.01	0.00	0.70	0.00	0.00	0.21	0.13	0.00	0.00	0.13	0.00
Bi	3.95	0.48	1.74	1.03	4.24	3.64	0.95	2.72	1.90	1.00	0.89	0.48
S	27.83	29.68	30.94	30.29	29.71	30.52	29.96	30.35	30.35	31.53	32.80	32.20
Se	0.36	0.29	0.19	0.68	0.26	0.26	3.05	0.43	1.26	0.99	0.79	1.49
Total	101.38	100.13	100.28	99.24	100.64	100.05	99.32	100.11	99.69	98.87	100.25	98.23
Sn	0.514	0.593	0.698	0.724	0.733	0.743	0.759	0.796	0.815	0.937	0.957	1.000
Pb	0.511	0.437	0.310	0.283	0.277	0.258	0.237	0.233	0.204	0.100	0.057	0.014
Cd	0.000	0.000	0.000	0.000	0.000	0.000	0.000	0.000	0.000	0.004	0.000	0.000
Ge	0.928	0.922	0.905	0.915	0.939	0.908	0.910	0.919	0.939	0.911	0.926	0.938
Sb	0.007	0.000	0.003	0.003	0.004	0.005	0.002	0.003	0.000	0.002	0.004	0.004
As	0.008	0.000	0.000	0.030	0.000	0.000	0.009	0.005	0.000	0.000	0.005	0.000
Bi	0.064	0.008	0.026	0.016	0.065	0.055	0.014	0.041	0.028	0.015	0.013	0.007
S	2.953	3.028	3.050	3.002	2.971	3.020	2.947	2.986	2.964	2.992	3.009	2.981
Se	0.016	0.012	0.008	0.027	0.011	0.010	0.122	0.017	0.050	0.038	0.029	0.056

Coefficients of empirical formula calculated on the basis 5 *apfu*

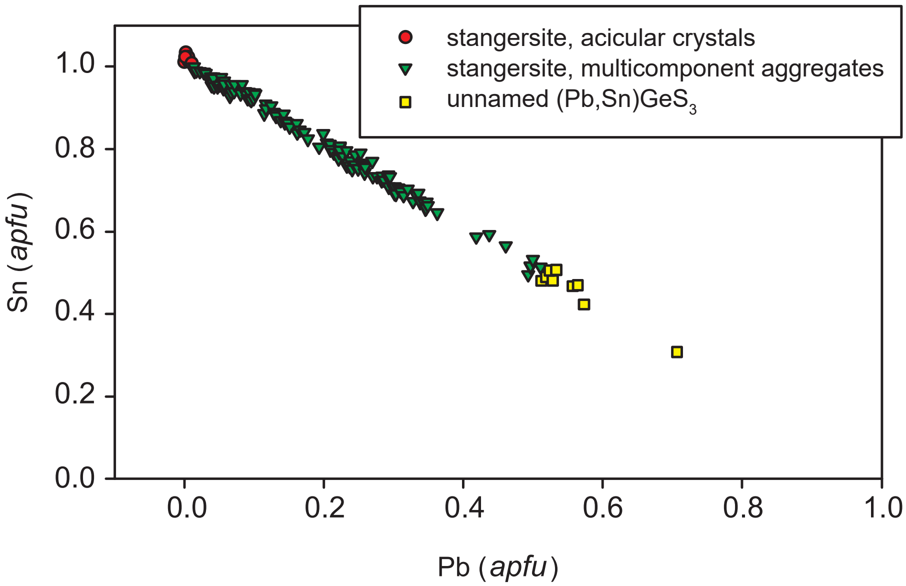

Fig. 4 The graph of Pb *vs* Sn (*apfu*) contents for phases of the $SnGeS_3$ (stangersite) - $PbGeS_3$ (unnamed) solid solution from Radvanice.

values (spectrophotometer MSP400 Tidas at Leica microscope, objective 100×, WTiC standard in the air) is given in Tab. 1 and plotted in Fig. 3.

4. Chemical composition

Samples of stangersite were analyzed with a JEOL Superprobe 733 electron microprobe in the wavelength-dispersive mode with an accelerating voltage of 20 kV, a specimen current of 20 nA, and a beam diameter of 1–2 µm. The following lines and standards were used: K_α: chalcopyrite (Fe, S); L_α: Bi (Bi), CdS (Cd), Cu_3AsS_4 (As), Ge (Ge), Sb_2Se_3 (Sb, Se), Sn (Sn); M_α: PbS (Pb). Raw intensities were converted into the concentrations automatically, using the on-line *ZAF* correction program supplied by JEOL. Detection limits were close to 0.01 wt. % for all measured elements. Absence of H_2O and CO_2 was confirmed by Raman spectroscopy and single-crystal X-ray study (Sejkora et al. 2001); lower totals of the EPMA analyses are caused by the acicular nature of the studied crystals.

Chemical composition of the acicular crystals of stangersite used for single crystal study (Tab. 2) corresponds to relatively pure Sn-end member with only minimal Pb content (Fig. 4), the empirical formula calculated from the mean of six analytical points on the basis of 5 *apfu* is as follows: $Sn_{1.02}Ge_{0.94}(S_{2.93}Se_{0.10})_{\Sigma 3.03}$ (Sejkora et al. 2001). The ideal formula, $SnGeS_3$, requires Sn 41.29, Ge 25.25, S 33.46, total 100 wt. %. The chemical composition of stangersite from multicomponent aggregates (Tab. 3) shows an extensive $PbSn_{-1}$ substitution (Fig. 4) covering practically the entire field of stangersite portion of the $SnGeS_3$–$PbGeS_3$ solid-solution. The composition of some aggregates with Pb > Sn (Tab. 4) already falls to the field of Sn-rich unnamed $PbGeS_3$ (Fig. 4): another potentially new mineral species. Although Bente (1981) described a continuous $SnGeS_3$–$PbGeS_3$ series formed at 450 °C, no members with higher Pb content were found

Tab. 4 Chemical data (in wt. %) for unnamed $(Pb,Sn)GeS_3$ mineral from Radvanice

	1	2	3	4	5	6	7	8	9
Sn	16.64	16.82	16.55	17.90	17.76	16.15	16.18	14.61	10.39
Pb	30.98	31.11	31.71	32.38	32.65	33.58	33.98	34.55	41.61
Cd	0.00	0.00	0.13	0.00	0.00	0.00	0.16	0.00	0.00
Ge	19.76	19.86	19.81	19.83	19.96	19.73	19.47	19.32	18.84
Sb	0.13	0.00	0.00	0.00	0.00	0.00	0.00	0.22	0.19
As	0.00	0.00	0.14	0.00	0.00	0.14	0.00	0.08	0.11
Bi	0.00	0.00	0.23	1.52	1.27	0.80	0.53	1.66	1.48
S	27.57	27.07	26.95	28.82	28.37	27.90	27.94	28.15	27.30
Se	2.90	2.85	2.96	0.43	0.34	0.74	0.73	0.71	0.90
Total	97.98	97.71	98.48	100.88	100.35	99.04	98.99	99.30	100.82
Sn	0.480	0.490	0.482	0.505	0.506	0.468	0.469	0.423	0.308
Pb	0.512	0.519	0.529	0.524	0.533	0.557	0.564	0.573	0.707
Cd	0.000	0.000	0.004	0.000	0.000	0.000	0.005	0.000	0.000
Ge	0.932	0.946	0.943	0.916	0.931	0.934	0.923	0.915	0.913
Sb	0.004	0.000	0.000	0.000	0.000	0.000	0.000	0.006	0.005
As	0.000	0.000	0.006	0.000	0.000	0.006	0.000	0.004	0.005
Bi	0.000	0.000	0.004	0.024	0.021	0.013	0.009	0.027	0.025
S	2.946	2.920	2.903	3.013	2.995	2.990	2.998	3.020	2.996
Se	0.126	0.125	0.129	0.018	0.015	0.032	0.032	0.031	0.040

Coefficients of empirical formula calculated on the basis 5 *apfu*

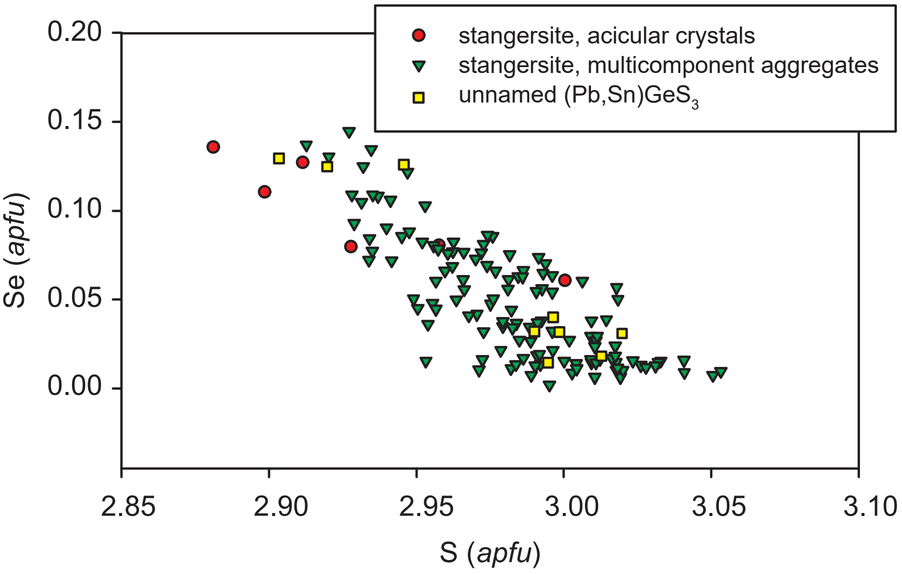

Fig. 5 The graph of S *vs* Se (*apfu*) contents for phases of the $SnGeS_3$ (stangersite)–$PbGeS_3$ solid-solution from Radvanice.

at Radvanice, indicating a lead deficit in the parental coal-fire gases. The regular small extent of SeS_{-1} substitution was determined in all the studied members of the $SnGeS_3$-$PbGeS_3$ solid-solution (Fig. 5); no correlation of Se/S and Pb/Sn ratios was observed.

5. Raman spectroscopy

The Raman spectra of stangersite were collected in the range of 2016–39 cm^{-1} using a DXR dispersive Raman Spectrometer (Thermo Scientific) mounted on a confocal

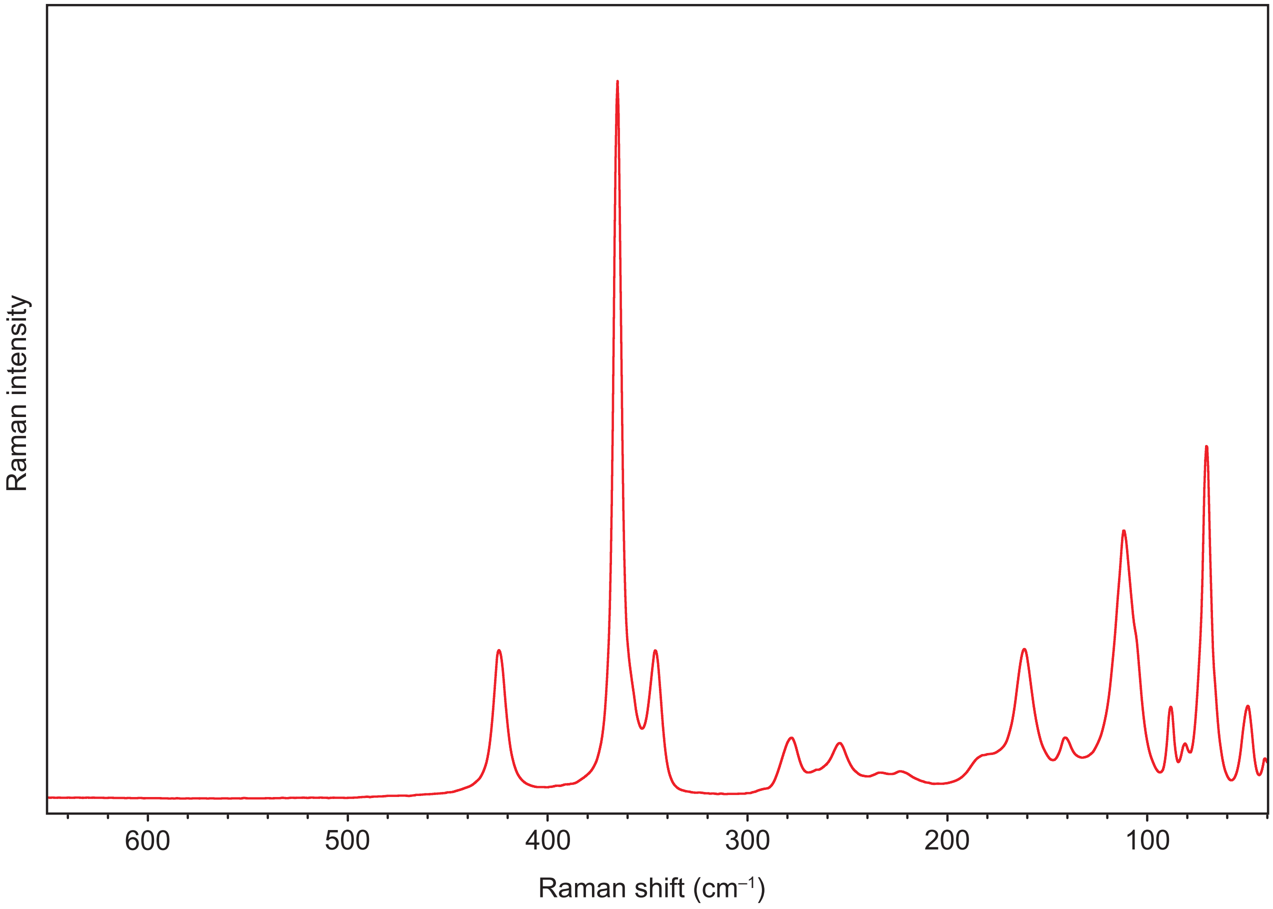

Fig. 6 Raman spectrum of stangersite in the range of 630–40 cm^{-1}.

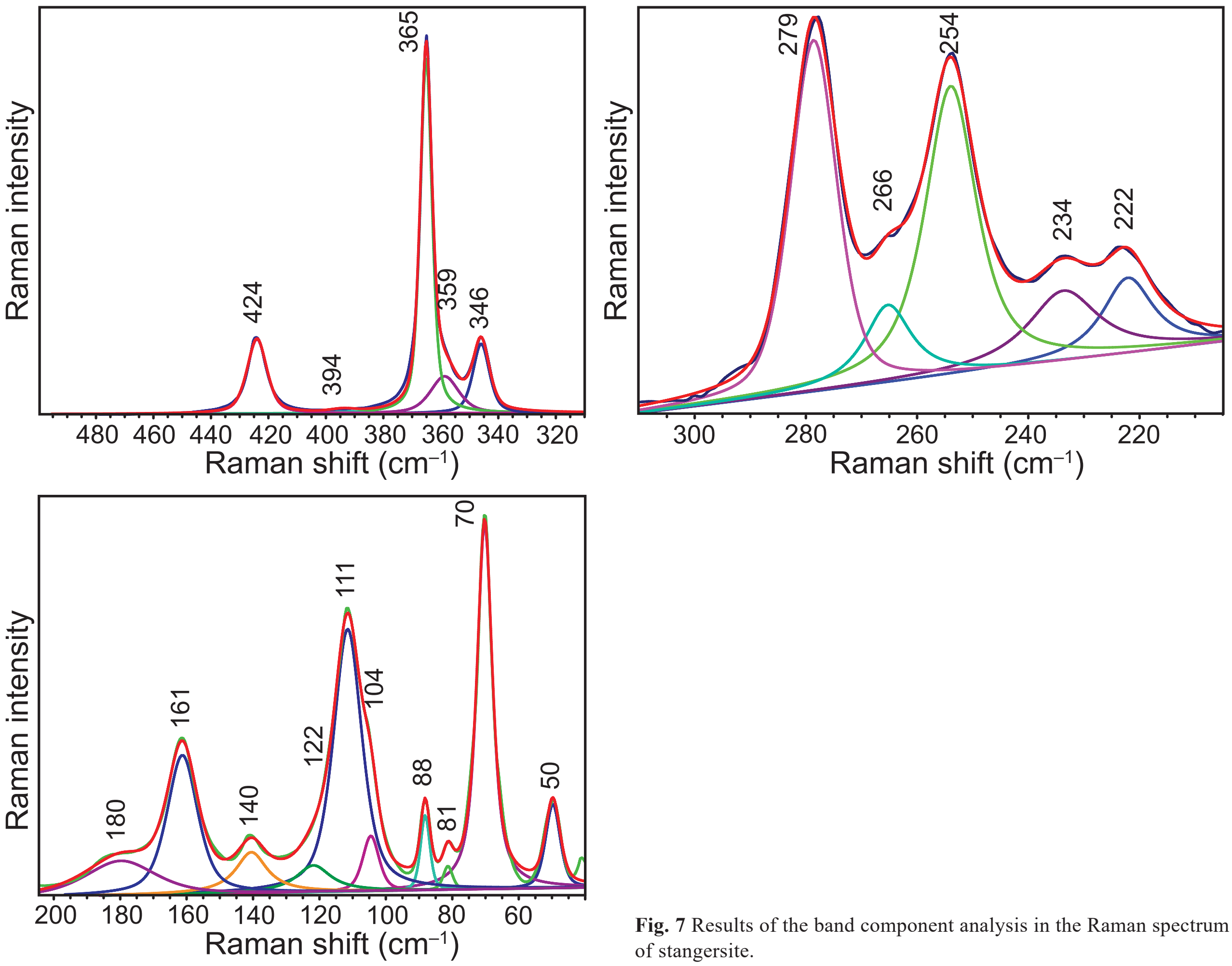

Fig. 7 Results of the band component analysis in the Raman spectrum of stangersite.

Olympus microscope. The Raman signal was excited by an unpolarised red 633 nm He-Ne gas laser and detected by a CCD detector. The experimental parameters were: 100× objective, 10 s exposure time, 100 exposures, 1200 lines/mm grating, 25 µm pinhole spectrograph aperture, and 2 mW laser power level. The possible thermal damage of the measured points was excluded by visual inspection of the excited surface after measurement, by observation of a possible decay of spectral features at the beginning of excitation, and by checking for thermal downshift of the Raman bands. The instrument was set up by a software-controlled calibration procedure using multiple neon emission lines (wavelength calibration), multiple polystyrene Raman bands (laser frequency calibration), and standardized white-light sources (intensity calibration). Spectral manipulations were performed using the Omnic 9 software (Thermo Scientific). Gaussian/Lorentzian (pseudo-Voigt) profile functions of the band shape were used to obtain decomposed band components of the spectra. The decomposition was based on the minimization of the difference in the observed and calculated profiles until the squared correlation coefficient (r^2) was greater than 0.995.

The full-range Raman spectrum of the stangersite is given in Fig. 6, the results of its decomposition in Fig. 7, and related tabularized values in Tab. 5. The experimental spectrum of stangersite from Radvanice agrees very well with published Raman spectra of synthetic $SnGeS_3$ (e.g., Stergiou et al. 2000; Inoue et al. 2001; Jakšić 2003, see Tab. 5). According to Bletskan et al. (2003), the intramolecular vibrations of the GeS_4 tetrahedra in the stangersite crystal structure can be described by irreducible representations of T_d factor-group as follows: $\Gamma_{in} = A_1 + E + 2F_2$. The A_1 representation corresponds to symmetric stretching vibration ν_1 (Ge–S). The F_2 representation is constituted by antisymmetric stretching ν_3 (Ge–S) and antisymmetric bending ν_4 (S–Ge–S) vibrations, both triply degenerated. Doubly degenerate E representation describes symmetric bending ν_2 vibration. For the "free" GeS_4 group, wavenumbers of vibrations (all Raman active) are as follows: $\nu_3 = 417$, $\nu_1 = 386$, $\nu_4 = 205$, and $\nu_2 = 170$ cm^{-1} (Pohl et al. 1973). As a result of GeS_4 deformation in the crystal field, the degenerated vibrations may be split into two (ν_2) or three (ν_3, ν_4) components. Observed bands in the range of 430–340 cm^{-1}

Tab. 5 Components of Raman spectrum of stangersite

Position [cm^{-1}]	FWHM [cm^{-1}]	$I_{rel.}$ [H %]	$I_{rel.}$ [A%]	Position[1] [cm^{-1}]	Position[2] [cm^{-1}]	Position[3] [cm^{-1}]	Assignment
424	8	20.2	31.6	424	424	423	ν_1 symmetric and ν_3 antisymmetric stretching vibrations of (GeS_4)
394	10	0.6	1.4	395			
365	5	100.0	100.0	365	364	363	
359	12	7.3	12.6	355			
346	7	18.7	24.0	346	346	345	
279	10	7.4	12.6				vibrations of Sn–S bonds
265	10	1.6	3.0				
254	11	6.1	13.5	252			
234	15	1.8	4.2	231	233		ν_4 antisymmetric bending vibrations of (GeS_4)
222	11	2.0	4.8	222	216		
180	25	4.2	14.9	182	175, 185		ν_2 symmetric bending vibrations of (GeS_4)
161	11	18.4	38.9	161	160	157	
140	11	4.7	11.3	139	139	136	external vibrations
122	13	1.8	3.8				
111	10	34.5	82.3	111	113		
104	6	7.2	9.5	106	106	104	
88	3	9.6	5.7	87	83	86	
81	3	3.3	3.2	80	81	79	
70	5	46.5	51.3	70	70, 72	67	
50	5	11.0	11.0	48	49, 50		

$I_{rel.}$ calculated from the band height (H) or area (A); position[1] – Inoue et al. (2001); position[2] – Stergiou et al. (2000); position[3] – Jakšić (2003)

are attributed to symmetric (ν_1) and antisymmetric (ν_3) stretching vibrations of corner-sharing GeS_4 tetrahedra; the low- and medium-intensity bands in the ranges of 240–220 cm^{-1} and 190–150 cm^{-1} are probably connected to antisymmetric bending ν_4 and symmetric bending ν_2 vibrations, respectively. Bands of the 290–240 cm^{-1} range may be attributed to vibrations of Sn–S bonds of SnS_5E octahedra (Bletskan et al. 2003). Bands below 150 cm^{-1} should correspond to the external vibrations.

6. Powder and single crystal X-ray diffraction

The X-ray powder diffraction data (Tab. 6) were collected with an HZG4/TuR diffractometer, Cu*K*α radiation, step-scanning of 0.05°/13 s, 11–68 ° 2θ range and published by Sejkora et al. (2001). Positions and intensities of diffractions were refined using the Pearson VII profile-shape function of the ZDS program package (Ondruš 1993). The following unit-cell parameters were refined by the least-squares program of Burnham (1962): $a = 7.257(3)$, $b = 10.232(5)$, $c = 6.863(4)$ Å, $\beta = 105.53(4)°$ and $V = 491.0(4)$ Å^3 (Sejkora et al. 2001).

The crystal structure of stangersite was solved by Sejkora et al. (2001) based on single-crystal X-ray diffraction data and refined to $R_1 = 3.28$ %. The refined unit-cell parameters $a = 7.2704(15)$, $b = 10.197(2)$, $c = 6.8463(14)$ Å, $\beta = 105.34(3)°$, $V = 489.5$ Å^3 and $Z = 4$ (Sejkora et al. 2001) are compared in Tab. 7 with published data of related phases. The calculated $a : b : c$ ratio is 0.7130 : 1 : 0.6714.

7. Crystal structure of stangersite

Sejkora et al. (2001) provided a basic structural description of stangersite. Here, we present an extended and novel description of the crystal architecture of this new mineral phase. Although, both cations occurring

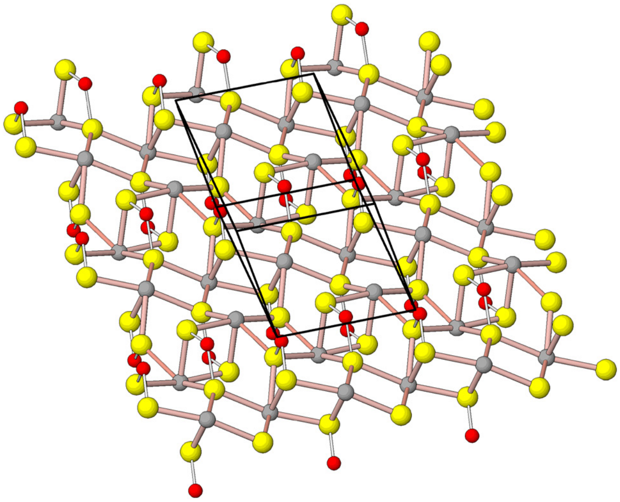

Fig. 8 Bond scheme of Sn^{2+} (grey) in the crystal structure of stangersite, with interconnection of tin coordinations in a corrugated layer and attachment of Ge atoms (red) to it marked.

Tab. 6 X-ray powder diffraction data (*d* in Å) for stangersite (Sejkora et al. 2001)

$I_{meas.}$	$d_{meas.}$	$d_{calc.}$	*h*	*k*	*l*
100	**7.006**	6.992	1	0	0
21	5.787	5.773	1	1	0
3	5.591	5.553	0	1	1
4	5.134	5.116	0	2	0
2	4.929	4.921	1	1	–1
49	**4.135**	4.129	1	2	0
20	4.059	4.046	0	2	1
9	3.939	3.939	1	1	1
26	3.786	3.781	1	2	–1
7	3.344	3.356	1	0	–2
11	3.310	3.314	2	2	–1
		3.308	2	1	0
3	3.273	3.277	1	2	1
1	3.185	3.190	1	1	–2
47	**3.077**	3.065	1	3	0
16	2.891	2.890	2	2	–1
		2.886	2	2	0
29	2.810	2.806	2	0	–2
		2.806	1	2	–2
38	**2.776**	2.777	0	2	2
69	**2.699**	2.698	2	1	1
2	2.668	2.664	1	3	1
17	2.626	2.629	1	1	2
17	2.447	2.441	2	3	0
3	2.402	2.404	1	4	0
12	2.380	2.386	0	4	1
29	2.345	2.346	3	1	–1
5	2.332	2.331	3	0	0
2	2.320	2.327	1	4	–1
15	2.274	2.273	3	1	0
1	2.242	2.230	1	1	–3
11	2.2015	2.194	3	0	–2
7	2.1805	2.1801	3	2	–1
31	**2.1213**	2.1210	3	2	0
14	2.0654	2.0657	2	4	–1
4	2.0229	2.0242	0	2	3
3	2.0229	2.0231	0	4	2
14	1.9948	1.995	3	1	1
15	1.8075	1.8089	2	3	2
5	1.7693	1.7669	2	5	–1
4	1.7481	1.7481	4	0	0
		1.7469	3	3	1
35	**1.7239**	1.7261	4	1	–2
		1.7231	4	1	0
3	1.7070	1.7100	4	2	–1
9	1.6985	1.7040	1	4	–3
		1.7023	3	0	2
18	1.6573	1.6568	4	2	–2
		1.6560	2	1	–4
4	1.6521	1.6530	0	0	4
		1.6513	2	1	3
4	1.6394	1.6385	2	4	2
1	1.6332	1.6354	1	5	2
3	1.5925	1.5920	3	4	1
15	1.5182	1.5209	4	2	–3
		1.5186	4	2	1
		1.5156	0	6	2
5	1.4430	1.4449	1	6	2
		1.4432	4	4	0
3	1.4203	1.4185	3	3	–4
21	1.3986	1.3984	5	0	0
		1.3983	4	0	2
3	1.3946	1.3941	5	2	–1

in the mineral can be present in nature both as divalent and tetravalent state, in the crystal structure of stangersite valence states are combined as divalent (Sn) and tetravalent (Ge). A combination of the coordination tetrahedra of Ge^{4+} with coordination pyramids/prisms of Sn^{2+} with a lone-electron pair (LEP) character leads to a unique crystal structure of $SnGeS_3$, shared only with $PbGeS_3$ (Ribes et al. 1974) in which similar bonding situation occurs.

Coordination polyhedron of Sn^{2+} is a broad-based square coordination pyramid, with Sn^{2+} slightly below the base and four Sn–S bonds in the base that are between 2.889 Å and 2.927 Å long (Fig. 8, Tab. 8). The pyramidal apex has a shorter Sn–S bond of only 2.637 Å. The lone electron pair of Sn is accommodated below the base of the pyramid, in a trigonal-prismatic space, created by the four sulfur atoms of the pyramidal base and two S atoms which are positioned across the space allocated to LEP's

Tab. 7 Unit-cell parameters for stangersite and synthetic $SnGeS_3$–$PbGeS_3$ phases (monoclinic, $P2_1/c$, $Z = 4$)

		a [Å]	*b* [Å]	*c* [Å]	*β* [°]	*V* [Å^3]
stangersite[1]	Sejkora et al. (2001)	7.2704(15)	10.197(2)	6.8463(14)	105.34(3)	489.5
stangersite[2]	Sejkora et al. (2001)	7.257(3)	10.232(5)	6.863(4)	105.53(4)	491.0
$SnGeS_3$	Žáček and Ondruš (1997b)	7.256(3)	10.227(6)	6.854(3)	105.469(5)	490.2(4)
$SnGeS_3$	Fenner and Mootz (1976)	7.269(1)	10.220(2)	6.873(2)	105.45(1)	492.1
$SnGeS_3$	Laufek et al. (2017)	7.2655(3)	10.2011(2)	6.8665(2)	105.42(1)	490.44
$PbGeS_3$	Ribes et al. (1974)	7.224(3)	10.442(2)	6.825(2)	105.7(1)	495.6

stangersite[1] – single-crystal X-ray data; stangersite[2] – powder X-ray data

Tab. 8 Selected interatomic distances [Å] and angles [°] for stangersite, with estimated standard deviations in parentheses. For each cation the distances from the central atom to the ligand are given in the diagonal. The angles between two ligands and the central atom are listed above, the distances between two ligands below the diagonal (Sejkora et al. 2001)

Sn1	S1	S1	S3	S3	S3	S2	S2
S1	2.637(1)	85.5(1)	84.2(0)	77.0(0)	70.2(0)	139.1(0)	155.1(0)
S1	3.754(2)	2.889(2)	168.3(0)	92.9(0)	97.0(0)	70.5(0)	119.4(0)
S3	3.725(2)	5.769(2)	2.910(2)	79.4(1)	84.7(1)	114.7(0)	71.1(0)
S3	3.464(2)	4.206(2)	3.723(2)	2.914(1)	144.8(1)	71.9(0)	100.4(0)
S3	3.209(2)	4.355(2)	3.932(2)	5.568(2)	2.927(2)	143.1(0)	103.9(0)
S2	5.784(2)	3.738(2)	5.429(2)	3.814(2)	6.124(2)	3.526(2)	58.9(0)
S2	6.078(2)	5.600(2)	3.814(2)	5.009(2)	5.142(2)	3.494(2)	3.584(1)

Ge1	S3	S1	S2	S2
S3	2.200(1)	103.6(1)	109.1(1)	120.1(1)
S1	3.464(2)	2.208(1)	112.1(1)	110.7(1)
S2	3.627(2)	3.700(2)	2.252(2)	101.5(1)
S2	3.862(2)	3.674(2)	3.494(2)	2.258(1)

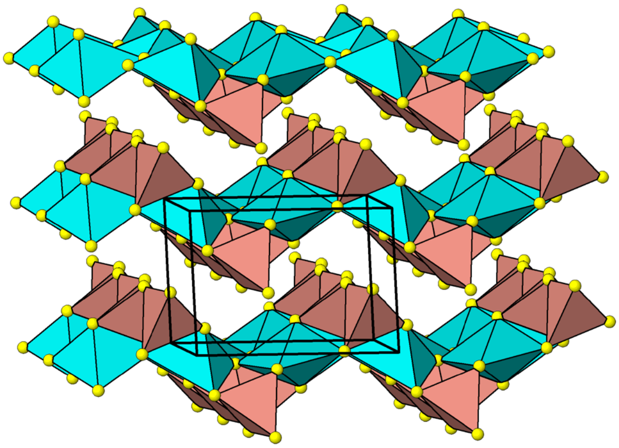

Fig. 9 Corrugated (100) layers of Sn^{2+} coordination polyhedra (monocapped trigonal prism, blue) and chains of Ge^{4+} coordination tetrahedra (mauve) in stangersite.

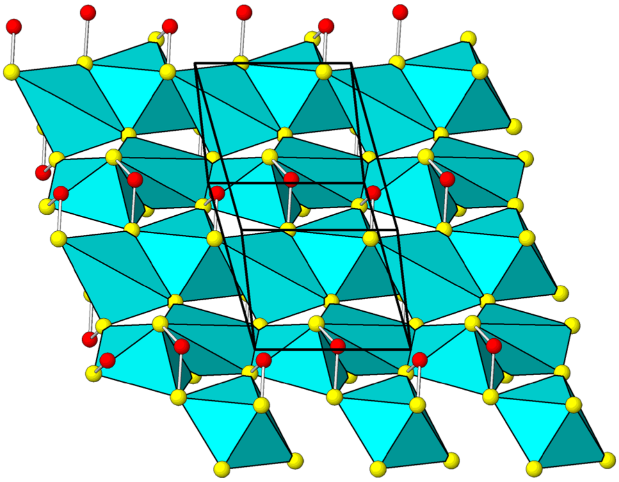

Fig. 10 Corrugated layer of SnS_5 coordination pyramids (blue) with Ge attached (red). Pyramids are interconnected *via* alternating edges and corners. The drawing program accentuates the slight break in the flat pyramidal bases.

of Sn^{2+}, at the distances of 3.526 Å and 3.584 Å (Fig. 9). The complete coordination of Sn^{2+} is a monocapped trigonal prism (CN 7) with the cation almost inserted into the prism cap.

Coordination pyramids of Sn occur in pairs, which are formed by sharing a common base edge. Vertices of these two pyramids are oppositely oriented, and each of them connects with a pyramid in adjacent pair, which is situated along [001], *via* a common oblique (inclined) pyramidal edge (Fig. 10). The near-equality of four basal Sn–S bonds (slightly elongated when facing the first type of the common edge) may be connected with the presence of the same charge load on all S atoms involved in the Sn layer: each of these S atoms has to accommodate three strong Sn–S bonds plus one Ge–S bond. Thus, the bond scheme is different from that observed in the structure of synthetic herzenbegite, SnS (del Bucchia et al. 1981).

The pyramidal pairs are placed in a herringbone scheme and are mutually related *via* a glide reflection plane (Fig. 10). The edge-connected [001] strings of them are interconnected only *via* corner atoms of the pyramids, not via edges. In this way, they form a strongly corrugated layer (Figs. 9, 10), which has only a weaker zig-zag contact between the adjacent, oppositely inclined strips of pyramids that form this layer.

The coordination tetrahedra of Ge (Fig. 9) are situated along, and close to, the above-mentioned glide planes. With the Sn portion of the structure, they share the ”contact” sulfur atoms, which are placed in the contacts of strings of Sn pyramids. Furthermore, they share with them also those S atoms, which form apices of Sn pyramids, and those S atoms which ‘close’ the trigonal prismatic spaces of lone electron pairs (LEPs) of Sn. The interspace created by the latter LEPs is sizable so that the LEP-populated layer is a (100) slab, which is void of atoms and is limited by tightly-bonded layers of Sn sulfide. It contains lone electron pairs and a system of parallel [001] Ge chains of tetrahedra (Fig. 9). The Ge

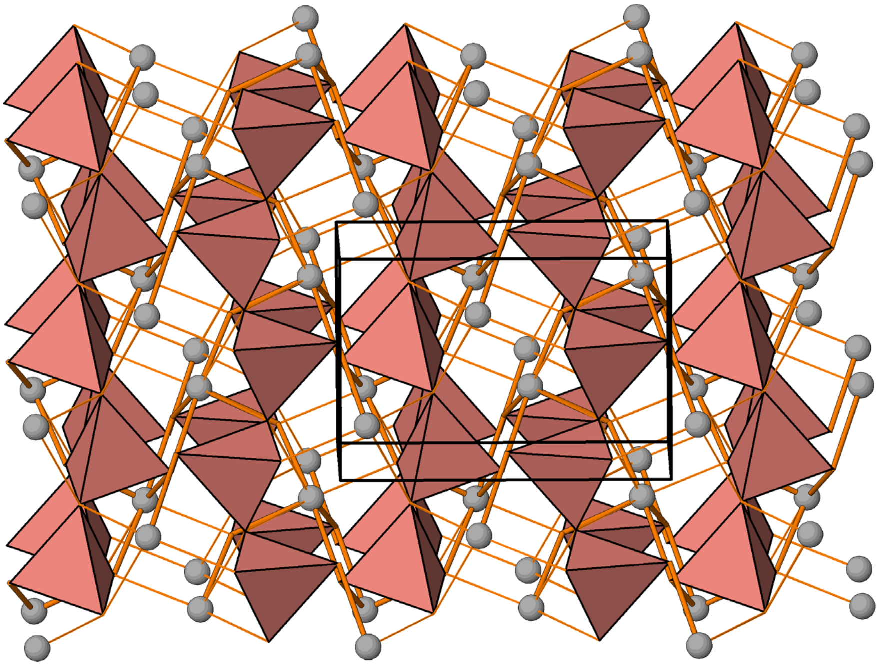

Fig. 11 Chains of Ge^{4+} coordination tetrahedra in the structure of stangersite.

tetrahedra are slightly asymmetric, with two bond lengths equal to 2.200 and 2.208 Å, and opposed by 2.252 and 2.258 Å. The inter-bond angles S–Ge–S vary in them between 101.5 and 120.1 ° (Tab. 8). The Ge tetrahedra are connected into completely stretched simple chains of tetrahedra (Fig. 11), in which they share corner anions with two tetrahedral neighbors and face the opposite [010] directions, alternatively.

Thus, although the structure may appear as composed of alternating Sn-rich and Ge-rich layers in some projections (e.g., in projection on (100) or along [110]), it is a misleading impression. It is a structure of corrugated tightly-bonded double-layers (analogous in principle to those of other lone electron pair compounds) with rods of tetrahedra in their crests (Fig. 9). Excellent (100) cleavage of stangersite is the result of this configuration.

Acknowledgements The study was financially supported by the Ministry of Culture of the Czech Republic (long-term project DKRVO 2019-2023/1.II.b; National Museum, 00023272). Both referees, Łukasz Kruszewski and Vladimír Žáček, same as handling editor František Laufek and the editor-in-chief Jakub Plášil, are highly acknowledged for comments and suggestions that helped to improve the manuscript.

References

Bente K (1975) Neue Erkenntnisse experimenteller Untersuchungen im kondensierten ternären System Ge–Sn–S. Fortschr Mineral 53(1): 5

Bente K (1981) Solid solution formation in the tin germanium sulfide ($SnGeS_3$) – lead germanium sulfide ($PbGeS_3$). Metall (Berlin) 35(2): 129–130

Bletskan DI, Kabacij VN, Sakal TA, Stefanovych VA (2003) Structure and vibrational spectra of $M^{II}A^{IV}B_3^{VI}$-type crystalline and glassy semiconductors. J Non-Cryst Solids 326: 77–82

Burnham CW (1962) Lattice constant refinement. Carnegie Institute Washington Yearbook 61: 132–135

Čadková Z (1971) The metal distribution in sediments of the Radvanice measures. Čas Mineral Geol 16(2): 147–157 (in Czech)

del Bucchia S, Jumas JC, Maurin M (1981) Contribution à l’étude de composés sulfurés d’étain (II): Affinement de la structure de SnS. Acta Crystallogr B37: 1903–1905

Dubanský A, Absolon K, Dvořáček (1988) Selenium from burning dumps of the Stachanov mine. Geol Průzk 3: 308–309 (in Czech)

Dubanský A, Langrová A, Dvořáček P, Čejka J, Kouřimský J (1991) Pyrometamorphic minerals from the Kateřina mine. Geol Průzk 6: 172–173 (in Czech)

Fenner J, Mootz D (1974) Die Kristallstruktur von $SnGeS_3$. Naturwissensch 61: 127

Fenner J, Mootz D (1976) Über Sulfide der vierten Hauptgruppe vom Typ $A^{II}B^{I}VS_3$ und die Kristallstruktur des $SnGeS_3$. Z Anorg Allg Chem 427: 123–130

Inoue K, Stergiou V, Raptis YS, Popović ZV (2001) Vibrational properties of $SnGeS_3$ under high pressure. J Phys Soc Jpn 70(7): 2168–2174

Jakšić ZM (2003) Temperature and pressure dependence of phonon frequencies in GeS_2, $GeSe_2$, and $SnGeS_3$. Phys stat sol (b), 239(1): 131–143

Kudělásek V (1959a) Trace elements of coal of the Intrasudetic Basin. Part I. Sbor věd Prací Vys Šk báň (Ostrava), Ř horn-geol 5(3): 319–347 (in Czech)

Kudělásek V (1959b) Trace elements of coal of the Intrasudetic Basin. Part II. Sbor věd Prací Vys Šk báň (Ostrava), Ř horn-geol 5(4): 457–479 (in Czech)

Laufek F, Veselovský F, Drábek M, Kříbek B, Klementová M (2017) Experimental formation of Pb, Sn, Ge and Sb sulfides, selenides and chlorides in the presence of sal ammoniac: A contribution to the understanding of the mineral formation processes in coal wastes self-ignition. Int J Coal Geol 176–177: 1–7

Miyawaki R, Hatert F, Pasero M, Mills SJ (2019) IMA Commission on New Minerals, Nomenclature and Classification (CNMNC), NEWSLETTER 50 New minerals and nomenclature modifications approved in 2019. Mineral Mag 83: 615–620

Nickel EH, Grice JD (1998) The IMA Commission on New Minerals and Mineral Names: procedures and guidelines on mineral nomenclature. Mineral Petrol 64(1–4): 237–263

Osner Z, Němec J (2002). Remediation of the burning waste bank of the mine Kateřina (Radvanice, Bohemia). Energie Kladno Ltd. (in Czech). Accessed on March 9, 2020, at http://slon.diamo.cz/hpvt/2002/sekce/zahlazovani/Z11/P_11.htm

Ondruš P (1993) A computer program for analysis of X-ray powder diffraction patterns. Materials Science Forum, EPDIC-2, Enchede, 133–136, 297–300

Öztunali Ö, Moh GH (1980) The Ge-Sn-S-O system. N Jb Miner, Abh 139(2): 118–121

Pohl S, Schiwy W, Weinstock N, Krebs B (1973) Darstellung, Schwingungsspektren und Normalkoordinatenanalyse der Ionen GeS_4^{4-} und SnS_4^{4-}. Z Naturforsch B28(9–10): 565–569

Ribes M, Olivier-Fourcade J, Philippot E, Maurin M (1974) Structure cristalline d'un thiogermanate de plomb à chaînes infinies $(PbGeS_3)_n$. Acta Crystallogr B30: 1391–1395

Sejkora J, Berlepsch P, Makovicky E, Balić-Žunić T (2001) Natural $SnGeS_3$ from Radvanice near Trutnov (Czech Republic): its description, crystal structure refinement and solid solution with $PbGeS_3$. Eur J Mineral 13: 791–800

Stergiou VC, Raptis YS, Popović ZV, Anastassakis E (2000) High-pressure Raman study of $SnGeS_3$. High Pressure Res 18: 189–194

Tásler R, Čadková Z, Dvořák J, Fediuk F, Chaloupský J, Jetel J, Kaiserová-Kalibová M, Prouza V, Schovánková-Hrdličková D, Středa J, Střída M, Šetlík J (1979) Geology of Czech part of the Intrasudetic Basin. Academia Praha (in Czech), pp 1–292

Tvrdý J, Sejkora J (1999) The burning coal mine dump and redeposition of toxic compounds during spontaneous thermic decomposition of coal matter. EKO – Ekologie spol 10(4): 11–15 (in Czech)

Tvrdý J, Sejkora J (2000) Recently formed mineral phases on burning mine dumps in Radvanice. Uhlí, rudy, geol průzk **7**(3): 19–24 (in Czech)

Žáček V, Ondruš P (1997a) Mineralogy of recently formed sublimates from Kateřina colliery in Radvanice, Eastern Bohemia, Czech Republic. Bull Czech Geol Surv 72 (3): 289–302

Žáček V, Ondruš P (1997b) Naturally occuring germanium compounds, $GeSnS_3$ and GeO_2 from Radvanice, Eastern Bohemia. Bull Czech Geol Surv 36 (2): 189–191

Žáček V, Skála R (2015) Mineralogy of Burning-Coal Waste Piles in Collieries of the Czech Republic. In Stracher GB, Prakash A, Sokol EV (Eds) Coal and Peat Fires: A Global Perspective, Volume 3 Case Studies-Coal Fires 109–159. Elsevier. Amsterdam